Stabilization of extensive fine-scale diversity by ecologically driven spatiotemporal chaos

Michael T. Pearce[a,1], Atish Agarwala[a,b,1], and Daniel S. Fisher[c,2]

[a]Department of Physics, Stanford University, Stanford, CA 94305; [b]Google Research, Mountain View, CA 94043; and [c]Department of Applied Physics, Stanford University, Stanford, CA 94305

Contributed by Daniel S. Fisher, April 30, 2020 (sent for review September 4, 2019; reviewed by Oskar Hallatschek and Boris I. Shraiman)

It has recently become apparent that the diversity of microbial life extends far below the species level to the finest scales of genetic differences. Remarkably, extensive fine-scale diversity can coexist spatially. How is this diversity stable on long timescales, despite selective or ecological differences and other evolutionary processes? Most work has focused on stable coexistence or assumed ecological neutrality. We present an alternative: extensive diversity maintained by ecologically driven spatiotemporal chaos, with no assumptions about niches or other specialist differences between strains. We study generalized Lotka–Volterra models with antisymmetric correlations in the interactions inspired by multiple pathogen strains infecting multiple host strains. Generally, these exhibit chaos with increasingly wild population fluctuations driving extinctions. But the simplest spatial structure, many identical islands with migration between them, stabilizes a diverse chaotic state. Some strains (subspecies) go globally extinct, but many persist for times exponentially long in the number of islands. All persistent strains have episodic local blooms to high abundance, crucial for their persistence as, for many, their average population growth rate is negative. Snapshots of the abundance distribution show a power law at intermediate abundances that is essentially indistinguishable from the neutral theory of ecology. But the dynamics of the large populations are much faster than birth–death fluctuations. We argue that this spatiotemporally chaotic "phase" should exist in a wide range of models, and that even in rapidly mixed systems, longer-lived spores could similarly stabilize a diverse chaotic phase.

ecology | diversity | chaos | spatiotemporal

Enormous diversity of species is one of the remarkable features of life on Earth. Once established by evolution, this diversity is traditionally explained in terms of niches and geographical separation. But spatial coexistence of a wide variety of species that seem to occupy similar niches is still a major puzzle (1).

Recent studies have found that even within individual microbial species [e.g., *Vibrio* (2) in the ocean, *Synechococcus* in hot springs (3, 4), *Staphylococcus epidermidis* on human skin (5, 6), *Neisseria* on the tongue (7), and *Bacteroides vulgatus* in guts (8)], many strains differing genetically on a broad spectrum of scales can coexist in nearby spatial locations. This fine-scale (or micro) diversity is especially surprising when strains mix together and are, hence, forced to compete. In some cases, the relevant mixing times are known: for the most abundant phytoplankton species, *Prochlorococcus*, which dominates tropical midoceans (9), a single sample contains hundreds of strains which diverged over timescales much longer than ocean-mixing times (10).

Why doesn't survival of the fittest eliminate fine-scale diversity on timescales that are long compared to generation or spatial mixing times, but still short compared to the evolutionary timescales over which the diversity must have evolved and been maintained? To understand this, is it necessary to interpret the strains, substrains, and sub-substrains as "ecotypes" (11) adapted to microniches and differing phenotypically in essential ways? Or might there be more general explanations? Any satisfying theory should lead to understanding of how the statistical structure of diversity—not just its existence—arises and is maintained by evolution.

Microbial diversity is often characterized by abundance distributions. Abundances typically range over many orders of magnitude extending down to very rare species and are often fit by power laws (12, 13). However, data on abundance distributions of within-species fine-scale diversity are limited (3, 4, 7). Furthermore, dynamical data are crucial to distinguish scenarios—as we shall discuss—but are much harder to come by due to the need for deeply sequenced time-series data, as in, e.g., refs. 6 and 7. Is local fine-scale diversity relatively stable? Or are blooms from low to high abundance and back down—observed in a variety of contexts (14, 15)—more the norm?

Theoretical ecologists have long endeavored to discover the ingredients necessary for diversity to persist in complex ecosystems. Most theoretical work has focused on "ecologically stable diversity" (reviewed in ref. 16). Common approaches include modeling interactions via competition for resources (17–21) and approximating interspecies interactions as "random" (22–27). A standard assumption is that species, or strains, compete with themselves and, hence, suppress their own population growth, more strongly than they interact with other strains: this is equivalent to assuming that each strain has its own niche. Niches may be a good starting point for modeling interactions among different species. But for closely related strains, there is no obvious reason why the interactions between "siblings" should be much stronger than between distant "cousins."

Significance

The diversity of living organisms is a fundamental feature of biology, yet still challenging to understand. Genomic data reveal that many closely related strains of bacteria can coexist for far longer than expected from "survival of the fittest." To explain this, is it necessary to assume a multitude of specialist niches, or are other mechanisms possible? We investigate, from simple but general models, an alternate scenario: coexistence of a large number of closely related strains in a chaotic state driven by ecological interactions. The chaos is characterized by local blooms and busts that are out of sync at different spatial locations. A natural example is multiple nonspecialist strains of a pathogen species infecting multiple strains of a host species.

Author contributions: M.T.P., A.A., and D.S.F. designed research, performed research, and wrote the paper.

Reviewers: O.H., University of California Berkeley; and B.I.S., University of California Santa Barbara.

The authors declare no competing interest.

See online for related content such as Commentaries.

[1]M.T.P. and A.A. contributed equally to this work.

[2]To whom correspondence may be addressed. Email: dsfisher@stanford.edu.

This article contains supporting information online at https://www.pnas.org/lookup/suppl/doi:10.1073/pnas.1915313117/-/DCSupplemental.

First published June 9, 2020.

The opposite extreme to niche-based approaches is the "neutral theory of biodiversity" (28–30), which posits that broad classes of species—such as all trees in some region—are ecologically equivalent. Species abundances fluctuate due to neutral birth, death, and migration processes instead of being stabilized by ecological interactions. The balance between these results in a broad distribution of abundances with a simple power-law tail (31) that compares well, at least semiquantitatively, to data on a variety of systems, such as marine plankton (13), diatoms of similar sizes (32), and trees in tropical forests (33).

But for microbial diversity, there is a major quantitative problem with neutral theory. The large sizes of microbial populations mean that birth–death fluctuations are far too slow to dominate population dynamics. And the short generation times mean that even tiny selective differences will be greatly amplified on modest timescales (34). To produce broad distributions from faster dynamics, recent work has generalized effective neutrality by considering species with different responses to a fluctuating environment, but still neutral time-averaged fitnesses (35, 36). But this does not solve the problem of fluctuating to extinction, or of how the average neutrality might arise.

A different approach, which we take here, is to ask whether ecological interactions and fitness differences can drive continually changing abundances in a state of "chaotic coexistence." As recognized early by May (37), a range of simple deterministic ecological models exhibit abundances that vary chaotically (38). It has been proposed that chaotic coexistence is important for plankton biodiversity (39, 40), and chaos has been demonstrated in a long-term experiment of an isolated planktonic food web (41). In nature, large changes in the relative abundances of viral and microbial strains have been observed in controlled, aquatic environments (42), and cycling between being abundant and rare is commonly observed in oceanic bacterial taxa (43). Might chaos be a generic feature of complex ecosystems (44, 45)? Can chaos promote or stabilize extensive diversity among close relatives? General theoretical analyses have shown that spatiotemporal environmental fluctuations can prevent extinctions and lead to coexistence (46, 47). And particular studies have found that chaos reduces extinctions in spatially extended populations (48, 49), but the chaotic population dynamics were put in by hand for a single species rather than arising from interactions. It is unclear if these mechanisms can stabilize extensive diversity.

It is often said that pathogens promote diversity (50). Pathogens surely contribute to continual evolution: a ubiquitous driving force is the advantage of evolving to "kill-the-winner" via predation, pathogenicity, or evolutionary arms races with relatives such as among *Streptoomyces* bacteria (51). Yet, it is far from clear whether evolutionary kill-the-winner dynamics enhances or decreases diversity.

Population dynamics driven by the advantages of doing well against currently abundant strains also occurs on ecological timescales; this will be our focus here. For pathogens, increasing abundance of a host strain can result in increasing abundance of particular pathogen strains: this limits the successful host population, driving it down, thereby limiting those recently successful pathogen strains as well. The original predator–prey Lotka–Volterra (LV) model demonstrated that such dynamics can lead to coexistence with periodic variations of the predator and prey populations. What about host–pathogen dynamics with many interacting populations? Models with specialist pathogens can lead to stable static communities (52, 53), as indeed does slight modification of the original LV model. Coupled predator–prey cycles have also been studied (54, 55), but, generically, multiple coupled cycles tend to lead to chaos.

A major drawback of most models of host–pathogen dynamics is that they do not account for broadly nonspecialist pathogens. Assuming all are specialists is equivalent to giving each strain its own niche. This may be reasonable for multispecies communities, but it is not for understanding within-species fine-scale diversity. Indeed, phages are often found to infect related, but phenotypically distinct, bacterial strains (56, 57). A crucial need for understanding fine-scale diversity is consideration of models with many strains of a single host species and many strains of a single pathogen species with broad, but varying, infectivity.

For microbial populations, evolutionary and ecological timescales overlap, and diversity is always being produced. However, there is an important question of principle—as well as, quantitatively, in practice: Does evolution generally lead to extensive spatially coexisting fine-scale diversity that would persist—in the absence of further evolution—for much longer than ecological timescales? A first step is to understand whether and how—without special assumptions—such diversity could persist. Can host–pathogen, or more general kill-the-winner, ecological dynamics stabilize fine-scale diversity on long timescales?

We analyze a general class of LV models and begin by investigating the nature of a diverse chaotic state that exists in a special case (58). However, in the generic case, chaos drives a cascade of extinctions that destroys the diversity. We then add the simplest form of spatial structure—identical islands with migration between them—and show that this leads to a robustly stable spatiotemporally chaotic "phase" that we argue should occur far more generally.

Models of Complex Diverse Ecosystems

We focus on generalized LV models widely used to model ecological interactions between species. For competing species, the dynamics of the population size, n_i, of species i is conventionally written in terms of a basic population growth rate, r_i, a carrying capacity κ_i, and a matrix W_{ij} of interactions between them:

$$\frac{dn_i}{dt} = n_i\left[r_i\left(1-\frac{n_i}{\kappa_i}\right)+\sum_{j\neq i} W_{ij}n_j\right]. \qquad [1]$$

This implicitly assumes that each species has its own "niche" and treats the interactions between species differently than interactions within species.

For closely related substrains, our focus, there is no a priori reason that interactions with the same strain are particularly different from with other strains. It is useful to separate out the overall constraints from use of the same resources, which will keep the total population of the K strains, $N\equiv\sum_{i=1}^{K} n_i$, approximately constant, and focus on the differences between them. We then write dynamics in terms of the fractional abundances (or frequencies) $\nu_i \equiv n_i/N$

$$\frac{d\nu_i}{dt} = \nu_i\left(s_i+\sum_{j=1}^{K} V_{ij}\nu_j - \Upsilon(t)\right), \qquad [2]$$

where the stabilizing term $\Upsilon(t)=\sum_i \nu_i(s_i+\sum_{j=1}^{K} V_{ij}\nu_j)$ keeps the total number fixed ($\sum_i \nu_i = 1$). We have dropped the explicit niche-like terms $r_i n_i/\kappa_i$ and treat the self-interactions V_{ii}—a priori of similar magnitude to the other interactions—on the same footing. The two models are equivalent if the general interactions between strains due to limited resources—parametrized by the average $\overline{W}=\frac{1}{K^2}\sum_{ij} W_{ij}<0$—is much larger than the differences $W_{ij}-\overline{W}$: this keeps fluctuations in the total population small. The interactions can be written in terms of the differences by $V_{ij}=N[W_{ij}-\frac{1}{K}\sum_j W_{ij}-\frac{1}{K}\sum_i W_{ij}+\overline{W}]$. Similarly, the selective differences—assumed much smaller than the average growth rate, $\bar{r}$—can be written as

$s_i = r_i - \bar{r} + [\frac{1}{K}\sum_j W_{ij} - \overline{W}]N$, which includes a part representing how strain i does against the average of the others.

Competition for resources will result in positive correlations between how strains interact with each other—e.g., between V_{12} and V_{21}—while direct one-on-one competition will result in anticorrelations: if strain 1 "beats" strain 2 so that $V_{12} > 0$, then 2 "loses" to 1 so that $V_{21} < 0$. Antisymmetric correlations of the interactions also occur for systems of hosts and pathogens in which a collection of strains of a pathogen infect a spectrum of strains of a host—e.g., intraspecies diversity within one phage and one bacterial species (56, 57). In terms of a population vector, $\begin{pmatrix} \boldsymbol{\nu}^{bacteria} \\ \boldsymbol{\nu}^{phage} \end{pmatrix}$, the interaction matrix has a block diagonal structure $\mathbf{V} = \begin{pmatrix} 0 & -\mathbf{F} \\ \mathbf{G} & 0 \end{pmatrix}$. For closely related strains, $\mathbf{F}$ and $\mathbf{G}$ will each consist of a constant part characteristic of the phage and bacterial species, plus small, strain-specific variations. The strain-specific parts of $\mathbf{F}$ and $\mathbf{G}^T$ (the transpose) will be positively correlated, since interactions that are better for the phage are worse for the bacteria and vice versa. *SI Appendix*, section 4 discusses how the results derived here can be generalized to the bacteria–phage model.

For simplicity, we focus on interactions between strains of a single species. Being sums and differences between similar interactions and similar growth rates, it is then natural to treat the V_{ij} and s_i as approximately random and characterize them by their statistical properties. The magnitudes of the V_{ij} set the timescale of the ecological dynamics. For most of our analyses, we will assume that the effects of overall fitness differences, the $\{s_i\}$, are much smaller than the differences in the influences of the interactions. (This corresponds to the assumption that generalists are hard to evolve.) We make the simplest choice for the distribution of the interactions: the $\{V_{ij}\}$, for $i \neq j$, are Gaussian distributed with mean zero, identical variance, and all covariances zero except across the diagonal. The ratio

$$\gamma \equiv \frac{\mathrm{E}[V_{ij}V_{ji}]}{\mathrm{E}[V_{ij}^2]} \quad \text{for} \quad i \neq j, \qquad [3]$$

with $-1 \leq \gamma \leq 1$, is the correlation coefficient between how the two strains affect each other: $\gamma = -1$ corresponds to an antisymmetric matrix, $\gamma = 0$ to independent elements, and $\gamma = 1$ to a symmetric matrix.

Niche-Like Interactions and Large Stable Communities. If, in spite of the similarities between strains, competition with others of the same strain are stronger—niche-like interactions—the diagonal terms would be negative on average, and we thus define $Q \equiv \mathrm{E}[-V_{ii}]/\sqrt{\mathrm{E}(V_{ij}^2)}$. An important point, however, is that for Q to affect the dynamics, the niche-like interactions must be much stronger than the interactions between different strains: as the sum over the (random) effects of all of the other strains will be proportional to $\sqrt{K}$, in order to substantially affect the ecological dynamics, Q must be of order $\sqrt{K}$. Most theoretical work, motivated particularly by competition for a mixture of resources (17, 18, 39, 59), has focused on such large Q (24, 60) and positive correlations between interactions, $\gamma > 0$ (20, 21, 25–27). In this regime, for a large number of strains, there is a unique stable, uninvadable community, corresponding to a stable fixed point of the dynamics, with a substantial fraction ($\mathcal{O}(K)$) of strains surviving and the other strains unable to invade. This occurs, for any γ, when $Q \geq Q_c(\gamma) = \mathcal{O}(\sqrt{K})$. For smaller Q, the fixed point destabilizes, and it appears that there is generally no large stable community [except for the special case of $\gamma = -1$ (58, 60)]. As we are interested in the interaction between large numbers of similar strains, we will mostly neglect the effects of niche-like interactions and set $Q = 0$.

What happens when there is no large stable community? Our focus will primarily be on $\gamma < 0$, for which dynamical ecologies are ubiquitous, as has been found in refs. 58 and 60. We first analyze the special case $\gamma = -1$. (The original LV model is this special case with $Q = 0$, $\gamma = -1$, and $K = 2$: it exhibits a family of periodic orbits.) With multiple types, the dynamics is chaotic. As we shall see, many aspects of the chaotic dynamics of this special model well characterize the behavior for a much broader range of parameters and models. Indeed the analysis of this special case serves as a needed framework for understanding chaotic dynamics more generally including, crucially, the effects of spatial structure.

Chaotic Ecological Dynamics

Perfectly Antisymmetric LV. The idealized model of perfectly antisymmetric interactions ($V_{ij} = -V_{ji}$) has very special properties, described in *SI Appendix*, section 3.A, which greatly facilitate its analysis. We here summarize its key features—see Figs. 1 and 4.

The antisymmetric model (ASM) has a family of stable chaotic states in which a fraction of the initial K strains—a unique set we call the "persistent strains"—coexist in a chaotic steady state, while the others have gone extinct and cannot reinvade. In steady state, each strain is characterized by its invasion growth rate, ξ_i—its bias for short—defined as its time-averaged growth rate when it is at very low abundance. If ξ_i is negative, strain i will go extinct. The behavior of the persistent strains, including their time-averaged abundances, $\langle \nu_i \rangle$, will be controlled by the magnitude of their particular positive ξ_i's. The scale of the ξ_i's, which we denote as $\hat{r}$, is $1/\sqrt{K}$ times the typical (rms) magnitude of the V_{ij}'s (roughly the sum of K terms, $V_{ij}\langle \nu_j \rangle$, of random sign with the $\langle \nu_j \rangle$ of order $1/K$ on average).

The effects of the interactions make the growth rates vary with time, so the logarithms of the fractional abundances $\ell_i \equiv \log(\nu_i)$ are the natural dynamical variables. In a chaotic steady state, the log-abundances of the persistent strains fluctuate over a range of width Θ, which depends on the initial conditions; this quantity (which turns out to be analogous to a temperature) parameterizes the family of chaotic steady states. The $\Theta = 0$ state corresponds to the unique fixed point of the persistent strains, with the other strains having gone extinct. For reasons that will become apparent later, we focus on large Θ, for which the frequency of the persistent strains fluctuate wildly. Each persistent strain occasionally "blooms" to high frequency. When it does so, it will have a large effect on strains that do better in its presence. But, as these other strains rise to high frequency themselves, the negative effects that they have on the first strain—implied by the antisymmetry of the interaction matrix—will cause its frequency to peak and start decaying, as illustrated in Fig. 1*B*. This "kill-the-winner" dynamics causes the peaks to typically last only for a short time, $\tau_{\mathrm{peak}} \sim 1/(\hat{r}\sqrt{\Theta})$. The typical growth rates of strains is of order $1/\tau_{\mathrm{peak}}$, which is much larger, by $\sim\sqrt{\Theta}$, than the time-averaged growth rates.

The wildly fluctuating growth rates for large Θ cause the log-abundances of the persistent strains to undergo superdiffusive random walks, seen in Fig. 1*A*. The statistical properties of these random walks turns out to be crucial and much more general than the ASM. Eventually, on a long timescale—of order the equilibration time of the chaotic state, $\tau_{\mathrm{eq}} \propto \Theta/\hat{r}$—the positive invasion rates of the persistent strains limit the range of their log-fluctuations, preventing their extinction. Strains with smaller positive ξ_i have $\log(\nu_i)$ fluctuating over a wider range and bloom less often, but the peaks of their blooms are statistically similar to the other persistent strains.

The essential nature of the ASM is only revealed by its dynamics, but a snapshot of the distribution of abundances of the

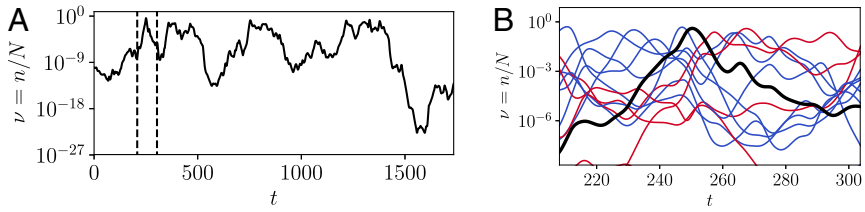

Fig. 1. Chaotic kill-the-winner dynamics of the perfectly ASM with no spatial structure. (*A*) Population dynamics of the fractional abundance (frequency), $\nu_i(t)$, of a single strain, out of a total of 301 persistent strains (of $K = 600$ initial strains). The range on the logarithmic scale is parametrized by the "temperature," Θ, which is determined by the initial conditions. Here, $\Theta = 40$, chosen unrealistically large to emphasize the different timescales, $\log(\nu_i)$ exhibits superdiffusive random-walk-like behavior over a wide range of timescales. Note the multiple peaks that occur before ν_i fluctuates down to low abundance, which typically takes a long time $\tau_{\text{eq}} \propto \Theta$. (*B*) Short time dynamics focusing on a high-abundance peak of one strain *i* (black). Its rise is due to the high abundance of several other strains, *j* (blue), with positive effects on strain *i* via $V_{ij}\nu_j > 0$. The high abundance of *i* then brings up populations of some other strains, *k* (red). Because of the antisymmetry, the effects of red strains on the black strain, via $V_{ik}\nu_k < 0$, cause negative feedback that drives the black population back down. Individual peaks typically last for short times $\tau_{\text{peak}} \propto 1/\sqrt{\Theta}$.

persistent strains shows their spread over a logarithmically wide range. As shown in *SI Appendix*, section 3.A, the full joint distribution of abundances can be found exactly. For large K, the abundances are essentially independent, and the probability density of the abundance of strain i has the simple form:

$$\begin{aligned}\rho_i(\nu_i)d\nu_i &\propto \nu_i^{-1+\mu_i/\Theta} e^{-K\nu_i/\Theta} d\nu_i \\ &\propto \exp(\ell_i\mu_i/\Theta - K\nu_i/\Theta) d\ell_i, \end{aligned} \quad \textbf{[4]}$$

with log-abundances $\ell_i \equiv \log \nu_i$ and the quantity $\mu_i \propto \langle \nu_i \rangle \propto \xi_i$, depending on the strain. For large Θ, the population of each strain is distributed roughly uniformly on a log scale up to a soft "ceiling" $\sim \Theta/K$, independent of i, while $\log(\nu_i)$ is exponentially suppressed at large negative values of order Θ/μ_i. In a snapshot of all of the strains, the (almost) independent sampling from the collection of the individual distributions is reflected in a broad distribution of the $\log(\nu_i)$, illustrated by a "rank-frequency" plot (see Fig. 4, dotted ASM curve). An important feature of this chaotic "phase" is that, in spite of the broad distribution of the abundances, the time-averaged abundances, $\langle \nu_i \rangle$, are not broadly distributed: each is proportional to the (small) fraction of the time that that strain is at high frequency.

Intriguingly, the form of Eq. **4**, as well as the joint distribution of all of the $\{\nu_i\}$ with fixed total population size (for which the exponential factors are replaced by $\delta(\sum_i \nu_i - 1)$), is identical to the frequency distribution from neutral ecological dynamics with genetic drift and random migration: specifically, with strain-i immigrants arriving at a low rate proportional to μ_i (61). However, the chaotic dynamics of the ASM is strikingly different from the stochastic neutral dynamics. It is hugely faster for large populations—for which the timescale of neutral dynamics is proportional to the population size, N. And the temporal correlations arising from the deterministic ecological dynamics are qualitatively different from those from stochastic birth–death fluctuations. We sketch derivations of these and other properties of the ASM in *Dynamical Mean-Field Theory*, with details relegated to *SI Appendix*, section 3.

Diverging Fluctuations for Near-Antisymmetric Interactions. When $\gamma > -1$, the stable high-diversity chaos of the perfectly antisymmetric model collapses. The roots of this instability can be understood in terms of the behavior of the ASM. When strain i rises to large frequency, some of the strains, j, that are driven upward by positive V_{ji}, will drive strain ν_i down via their typically negative V_{ij}. The average strength of this kill-the-winner effect is set by the negative correlations between V_{ij} and V_{ji}, parametrized by γ, as well as by how far the log-abundances of the other strains need to rise by in order to drive strain i down. For $-\gamma < 1$, the kill-the-winner effect is weaker; thus, the peaks are higher and last longer. These larger peaks mean that the instantaneous growth rates (which are set by the highly abundant strains) change more slowly. This causes all strains to fluctuate over a larger range of log-abundances, and it takes longer for these strains to again bloom from low abundance to high. This feedback loop, analyzed in *SI Appendix*, section 3.F, continues to amplify the fluctuations, eventually driving extinctions, as shown in *SI Appendix*, Fig. S3.

Our analyses have focused on γ substantially negative. But in parallel work, Roy et al. (62) have studied the case $\gamma = 0$ and niche interactions $Q < Q_c(\gamma)$; they also find diverging chaos driving extinctions. We conjecture that stable high-diversity chaos is not possible anywhere in the $Q - \gamma$ parameter space, except for the special point $\gamma = -1$, $Q = 0$.

Chaotic Coexistence Stabilized by Migration. In a well-mixed population, ecological chaos for $\gamma > -1$ causes larger and larger fluctuations to low abundance, quickly leading to a cascade of extinctions. In order to prevent extinctions, an influx of new individuals of each strain is needed. The simplest model with this property—widely used for island biogeography (63)—considers a "mainland" with a pool of each strain from which there is a low rate of migration to the "island" being studied. If the migration is not too small and the populations are large, the dynamics are approximately deterministic, and chaos on the island will be stabilized. But this begs the question of how the mainland diversity is stabilized: What prevents global extinctions?

Instead of a mainland, we consider the simplest spatial model: a large set of I islands (or "demes") with migration between all of them. For each strain, this presents a large pool of potential immigrants, but allows for global extinction of its whole pool. The islands are identical (strains interact via the same matrix V on each), and there is no additional spatial structure: migration rates between any pair of islands are all of the same with rate m per individual out of each island. The dynamics of the abundance, $\nu_{i,\alpha}(t)$, on island α follows Eq. **2**, with an additional term for the net migration of individuals, $m(\bar{\nu}_i - \nu_{i,\alpha})$, where $\bar{\nu}_i(t) \equiv \frac{1}{I}\sum_{\alpha=1}^{I} \nu_{i,\alpha}(t)$ is the average over all of the islands of the abundance of strain i. The local stabilizing term, $\Upsilon_\alpha(t)$, keeps the total population on each island, separately, equal to N (i.e., for each α, $\sum_i \nu_{i,\alpha} = 1$).

Local extinctions occur when the population of a strain on an island decreases below one individual, i.e., when its fractional abundance $\nu_{i,\alpha}$ falls below an extinction threshold of $1/N$. But even with small migration rates, $m \ll \hat{r}$, the inflow of migrants can compensate for a negative local growth rate to keep the local abundance on an island above or near a minimum size, $\nu_i^{\text{mig}} \sim m\bar{\nu}_i/\hat{r}$, which we call the "migration floor." We consider migration rates such that the migration floor for typical persistent types is well above the extinction threshold. (Note

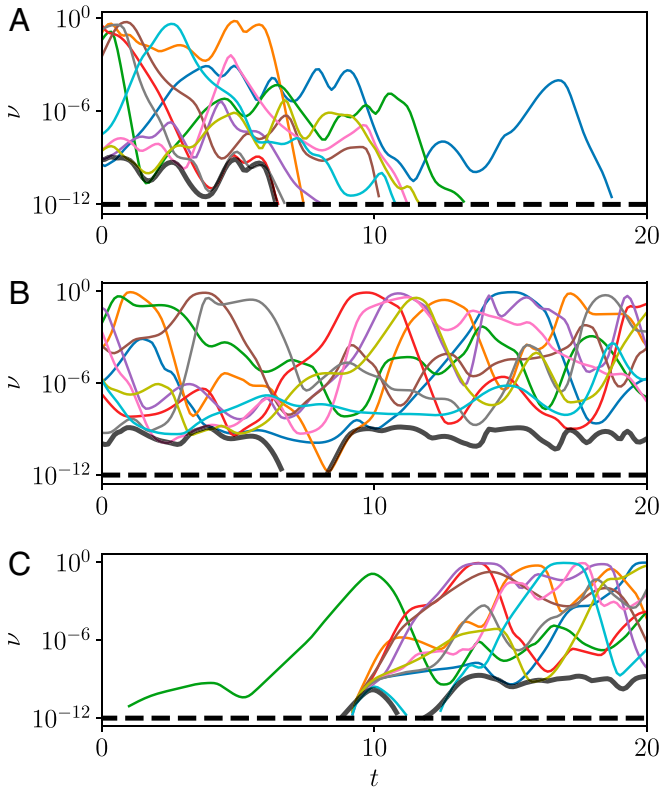

Fig. 2. Abundance trajectories of a single strain across $I = 10$ islands. ($K = 75$ initial strains, $\gamma = -0.8$, $N = 10^{12}$, $m/\hat{r} = 2 \cdot 10^{-8}$.) Black lines show the migration floor at which the local populations are stabilized by migration from other islands, and the dashed line is the boundary for extinctions, $\nu = 1/N$ (i.e., one individual). (*A*) For this strain, a global extinction results from a cascade of local extinctions due a shortage of large blooms on enough islands. (*B*) A persistent strain in steady state. Local extinctions can occur when the migration floor, and hence some local populations, drops below $\nu = 1/N$. But migration prevents local extinctions from becoming a global extinction, as long as a bloom to high abundance is occurring on at least one island. (*C*) An invasion can start from a small local population on one island which, if lucky, initiates a bloom from which migrants establish populations on other islands and leads to long-term persistence.

that this is the opposite limit usually studied in neutral island bio-geography.) Since birth–death fluctuations are negligible except when ν_i^{mig} is anomalously small, one can treat the population dynamics as essentially deterministic, including during extinctions when $\nu_i^{\mathrm{mig}}(t)$ falls below $1/N$, and during reestablishments when migration and a positive growth rate bring $\nu_i^{\mathrm{mig}}(t)$ back above $1/N$.

Even with migration, some strains go extinct globally, as shown in Fig. 2*A*. But for a wide range of m, a majority of strains persist for long times in spite of some local extinctions; Fig. 3. The dynamics of the abundances of a single persistent strain across all of the islands is shown in Fig. 2*B*. While much of the time, the population on an island is near the migration floor, as indicated, on each island there are local blooms up to high abundance which produce enough emigrants to other islands to avoid local extinctions and enable later blooms on the other islands. Indeed, even a small initial population on a single island can bloom and seed other islands, leading to long term persistence, as shown in Fig. 2*C*. Global extinctions only occur when such blooms are too rare.

A crucial feature that enables global persistence is that the chaos on different islands is desynchronized. This occurs if the migration rate is less than the largest Lyapunov exponent on a single island (64): $m \ll \hat{r}$ is sufficient. The desynchronization leads to a spatiotemporally chaotic steady state in which the island average $\bar{\nu}_i(t)$ of a persistent strain undergoes only small fluctuations. In steady state, the time-average abundance of a persistent strain, i, will be the same on each island: $\langle \nu_{i,\alpha} \rangle = \bar{\nu}_i$ for each α. Which strains persist, and their average abundance if they do, is determined (as for the ASM) by their bias, ξ_i—their average single-island invasion growth rate.

The key feature that makes coexistence of a majority of the strains possible is that even strains with negative ξ_i—which would go rapidly extinct in a well-mixed population—can nevertheless persist because of their occasional blooms. Although on each island, the growth rate of such strains will be negative for long periods of time, blooms to high abundance on some (not-too-tiny) fraction of the other islands can keep the island average $\bar{\nu}_i$ large enough at all times to rescue local populations from extinction.

A snapshot of the abundances of all of the strains on a single island, Fig. 4, shows the broad spread of the log-abundances $\log(\nu_{i,\alpha})$. Much of the time, the abundances of strains with negative ξ_i hover around the migration floor. This leads to a concentration at the low-abundance end (in contrast to the ASM; shown dashed for comparison). At intermediate and high abundances, the distributions for different γ are similar, with $\log(\nu_i)$ distributed approximately uniformly (as in the ASM distribution of Eq. **4**), but here over a range $\log(\nu^{\mathrm{peak}}/\nu^{\mathrm{mig}}) \approx M \equiv \log(\hat{r}/m)$. Indeed, to distinguish the distributions for different γ, or from the ASM, a very low-abundance detection threshold is needed: from a snapshot it is hard to estimate the total persistent diversity. However, averaging abundances over islands, or over very long times, reveals many more persistent strains with their average abundances, $\{\bar{\nu}_i\}$, relatively narrowly distributed (Fig. 4, *Inset*).

Much of our theoretical understanding of the spatiotemporal chaos is obtained from the limit of many strains and many islands, for which the dynamical mean-field analysis developed

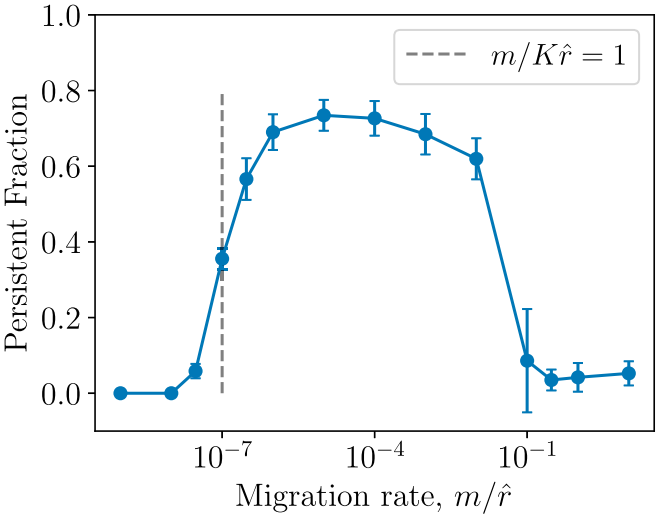

Fig. 3. Persistent fraction of strains vs. migration rate. Out of $K = 100$ strains, the fraction that are persistent is greatest for intermediate migration rates. For $m/\hat{r} = 10^{-1}$, islands become synchronized, leading to a large loss of diversity, while for $m/\hat{r} = 10^{-7} = K/N$ (dashed line), the migration floor for a typical strain drops below one individual. Results are averaged over 20 instantiations of V_{ij} with population per island, $N = 10^9$, and $\gamma = -0.8$. To extrapolate to the limit of many islands, simulations were run for $I = 30$ islands without an extinction threshold, and the persistent strains were defined as those with a migration floor, $m\bar{\nu}_i/\hat{r}$, greater than $1/N$.

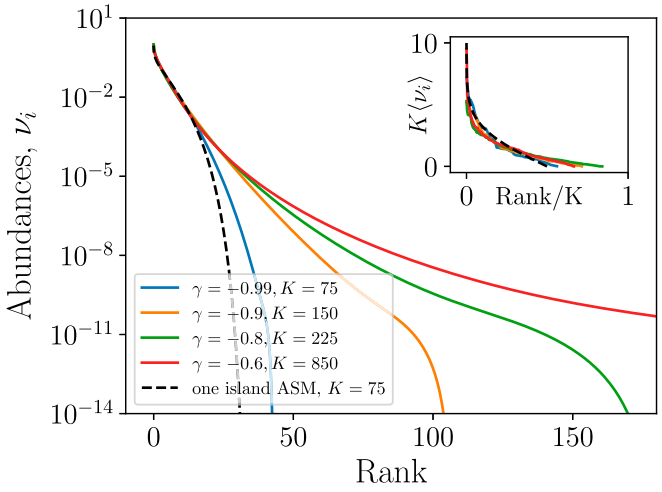

Fig. 4. Rank-frequency plots for island model ($I = 24$ islands, migration rate $m = 2 \cdot 10^{-9}$, and various γ). "Snapshots" of the fractional abundances, ν_i, on a single island are broadly distributed on a logarithmic scale. The initial number of strains, K, is chosen so that the number of strains in the distribution at large and intermediate abundances—the most readily observable part—is similar for each γ. The constant slope for this part of the distribution implies that $\log \nu_i$ is uniformly distributed over that range, as also found in neutral models. Stabilization via migration from other islands results in clustering at low abundances around the migration floor $\nu^{\text{mig}} \approx m/\sqrt{K}$, of order 10^{-10} for the $\gamma = -0.9$ and -0.8 curves. Time-averaged abundances $\langle\nu_i\rangle$ show much narrower distributions (*Inset*; on linear scale), similar for all γ when adjusted for different K. The $\gamma = -0.99$ curve is close to the single-island ASM ($\gamma = -1$; dotted line) with the same K and with the "temperature" scale Θ chosen, for comparison, equal to $M \equiv \log(1/m\sqrt{K})$. But with migration between islands, additional strains persist, even for γ very close to -1 (blue).

in the next section is asymptotically exact. But understanding the statistical dynamics of the blooms in this limit is the key to understanding how and for how long strains with negative ξ_i can persist with a finite number of islands. With finite I, persistent strains will have periods of bad luck when no blooms occur on any island for an extended period: this can cause the island average, $\bar{\nu}_i(t)$, to fluctuate down enough to cause global extinction. Since each island's dynamics is roughly independent, the probability of a strain having no blooms across all I islands for an extended period is exponentially small in I, as analyzed in *Global Extinctions*. Strains can thus persist for exponentially long times, as shown in Fig. 5. Quantitatively,

$$T_i^{\text{persist}} \sim \exp(I/I_X(\xi_i)), \qquad [5]$$

with the function $I_X(\xi_i)$ parametrizing the degree of stability of strain i: this is as a function of the strain's invasion growth rate, ξ_i; Eq. **14**.

Dynamical Mean-Field Theory. The dynamics of the multistrain models are intractable, even for the special single-island ASM. However, we can take advantage of the large number of strains and the random nature of the interactions among them and use an approach developed for other random systems: dynamical mean-field theory (DMFT) (65). This is valid when V_{ij} is a very large random matrix—in our case with elements independent and identically distributed except for the cross-diagonal covariance parameterized by γ (Eq. **3**). The DMFT approach approximates the population dynamics of a strain of interest, i, which is deterministically driven by its interaction with many others, by an effective stochastic integro-differential equation for that strain alone on a single island:

$$\frac{d\nu_i}{dt} = \nu_i \left(s_i + \zeta_i(t) + \gamma \int_0^t R(t,t')\nu_i(t')\,dt' - \Upsilon(t) \right) + m(\bar{\nu}_i(t) - \nu_i), \qquad [6]$$

with $\bar{\nu}_i(t)$ the average over the other islands. (Without spatial structure, the last term is absent.) For most analyses, we will not include the effects of the selective differences, s_i: these are addressed in the *Discussion* and *SI Appendix*, section 3.B.

The crucial features are the effects on strain i of interactions with the other strains: these have two contributions. The first, and intuitive, part, is an effectively random time-dependent drive—i.e., instantaneous growth rate—$\zeta_i(t)$, from the cumulative effects of all of the other strains, $\sum_{j\neq i} V_{ij}\nu_j$, *when strain* i *is absent*, $\nu_i(t) = 0$. The dynamics of strain i when invading (or at low abundances for an extended time) are set exclusively by $\zeta_i(t)$. Due to the K weakly correlated contributions with random coefficients, the drive, $\zeta_i(t)$, will be essentially Gaussian with mean (across strains) zero and temporal correlations reflecting the dynamics of the other strains:

$$\langle \zeta_i(t)\zeta_i(t') \rangle = \sum_{j,k} V_{ij}\nu_j(t)\, V_{ik}\nu_k(t') \approx \sum_j \nu_j(t)\nu_j(t') \equiv C(t,t'), \qquad [7]$$

(using $\mathrm{E}[V_{ij}\, V_{ik}] = \delta_{jk}$) and defining the correlation function, $C(t't')$. For large K, the correlations between the drives on different strains are essentially independent, and DMFT is asymptotically exact.

The second effect of interactions occurs when ν_i rises to high abundance and affects the other strains. For large K, its effect will be a small perturbation, $h_j(t) = V_{ji}\nu_i(t)$, to the growth rate of strain j, which is smaller by a factor of $\sqrt{K}$ compared to the total drive on strain j. The linear response of strain j, $\delta n_j(t)$, to $h_j(t')$ at earlier times t'—proportional to the functional derivative $\delta\nu_j(t)/\delta h_j(t')$—will give a small, but systematic, additional contribution, $V_{ij}\delta\nu_j(t)$, to the growth-rate strain i. The net effect

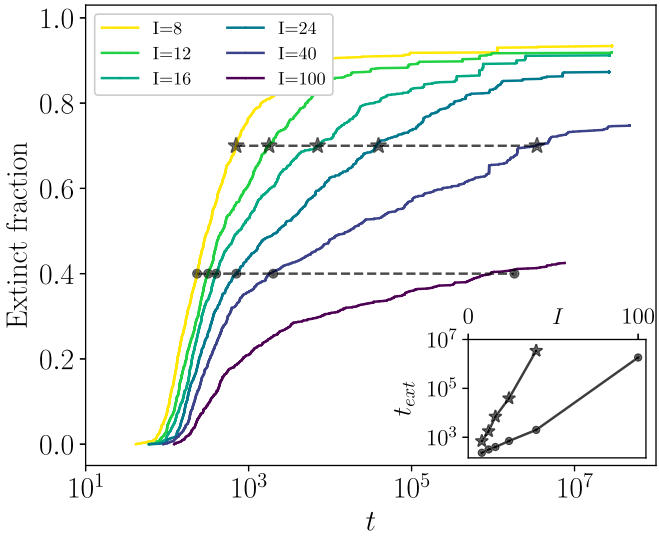

Fig. 5. Extinct fraction vs. time: after rapid, essentially deterministic, initial extinctions, the remaining strains persist for long periods of time. (*Inset*) With an increasing number of islands, I, more strains survive for long periods, and the typical time taken before a fixed fraction of strains have gone extinct (horizontal lines for fractions 0.4 and 0.7) increases exponentially with I. Data are from long simulations of 10 replicates with $K = 100$ starting strains, $m/\hat{r} = 2 \cdot 10^{-8}$ ($M = 18$), $N = 10^{13}$, and $\gamma = -0.8$.

back on $\nu_i(t)$ from its effects on others at earlier times is, since $\mathrm{E}[V_{ij}\,V_{ji}]=\gamma$, determined by

$$\sum_j V_{ij}\frac{\delta\nu_j(t)}{\delta h_j(t')}\,V_{ji}\approx\gamma\sum_j\frac{\delta\nu_j(t)}{\delta h_j(t')}\equiv\gamma R(t,t'), \qquad [8]$$

with $R(t,t')$ the "response function," which, together with $C(t,t')$, must be determined self-consistently. Unfortunately, in contrast to many studied problems, there are no closed equations for the response and correlation functions, so we must analyze the stochastic single-strain dynamics directly.

DMFT for Antisymmetric Single-Island Model. The mathematical analysis of *SI Appendix*, sections 3.D and 3.E reveals the full quantitative properties of the self-consistent solution of the DMFT for the single-island ASM. But the key features of the strongly chaotic steady state for large Θ are relatively intuitive once one knows it exists: this relies on the special properties elucidated in *SI Appendix*, section 3.A.

Each persistent strain has a—distinct—nonzero average abundance, $\langle\nu_i\rangle$. In steady state, the correlation function, $C(t-t')$, depends only on time differences and at long times decays to $C(t-t'\to\infty)=\sum_i\langle\nu_i\rangle^2$. Thus, the "drive" on each strain can be decomposed as $\zeta_i(t)=\langle\zeta_i\rangle+\eta_i(t)$ into a dynamic part $\eta_i(t)$ having zero time average and the same covariance for each strain, $\mathrm{E}[\eta(t)\eta(t')]=C(t-t')-C(\infty)$, and a static part $\langle\zeta_i\rangle$ which varies from strain to strain. For the ASM, the invasion growth rate, or bias, $\xi_i=s_i+\langle\zeta_i\rangle-\langle\Upsilon\rangle$ is simply $\langle\zeta_i\rangle$ since the stabilizing term is identically zero, $\Upsilon=0$, and we are, for now, not including the selective differences s_i.

Only strains with positive bias persist. Thus, since the $\{\xi_i\}$ are Gaussian distributed with mean zero, half the strains will go extinct. Time-averaging $d\log(\nu_i)/dt$ in Eq. **6** shows that the average abundance of the persistent strains is simply proportional to their bias

$$\langle\nu_i\rangle=\xi_i/\chi, \qquad [9]$$

with the static response $\chi\equiv\int_{-\infty}^{t}R(t-t')dt'$. The self-consistency conditions on the static response χ and $C(\infty)=\sum_i\langle\nu_i\rangle^2$ fix the values of $\chi\sim1/\sqrt{K}$ and the variance of ξ_i, of order $1/K$. The more general case including selective differences, s_i, is analyzed in *SI Appendix*, section 3.B.

Kill-the-winner feedback is represented by (for $\gamma=-1$) the $-\int R\nu_i$ term of Eq. **6**, which prevents each ν_i from getting too large and determines the shape of the resulting peaks: these typically reach an abundance $\nu_i\sim\Theta/K$ and last a time $\tau_{\mathrm{peak}}\sim\sqrt{K/\Theta}$ (*SI Appendix*, section 3.E). Far away from its own peaks, when $\nu_i(t)$ has been small for a long time, the effects of the feedback are negligible, and $\log(\nu_i(t))$ undergoes a random walk driven by its $\eta_i(t)$, typically of order $\sqrt{\Theta/K}$, plus a smaller (by $1/\sqrt{\Theta}$) upward bias ξ_i.

Since abundances are distributed broadly on a log scale, the sums over strains determining $C(t,t')$ and $R(t,t')$ are dominated by the roughly K/Θ strains that are peaking at any time. (Validity of the DMFT therefore requires that $K\gg\Theta$, so that many strains contribute to the sums.) The correlation function is proportional to the probability that a strain is peaking at both t and t'. If $\ell_i(t)$ behaved like a normal random walk, from a peak at t', it would return to near zero—and, hence, a peak—with probability decaying as $1/\sqrt{t-t'}$, but that would make $C(t-t')$, and thus the correlations of the dynamical noise, $\eta_i(t)$, long-range in time. Thus, the ansatz of a normal random walk is inconsistent. In *SI Appendix*, section 3.D, we show that the self-consistency condition for $C(t-t')$ makes the temporal-clustering statistics of the peaks cause a power-law decay of the correlations, $C(t-t')\sim|t-t'|^{-2/3}$, for a wide range of times.

The random walk of $\log(\nu(t))$ is therefore superdiffusive: in a time interval t, $\log(\nu)$ typically changes by

$$\Delta\ell(t)\sim(\Theta/K)^{1/3}t^{2/3}. \qquad [10]$$

On longer timescales, $\tau_{\mathrm{eq}}\sim\Theta\sqrt{K}$, the effects of the bias are felt, and the fluctuations of $\log(\nu_i(t))$ are gradually cut off at very low log abundances, reflected in the snapshot abundance distributions (Eq. **4**).

With $\gamma>-1$ on a single island, the chaos is no longer stable. A quantitative analysis can be carried out when $\gamma=-1+\epsilon$ with ϵ small (*SI Appendix*, section 3.F) using the DMFT solution for the ASM to describe how the temperature scale Θ gradually increases with time (*SI Appendix*, Fig. S3).

Analysis of Spatiotemporal Chaos

We now analyze the spatiotemporally chaotic behavior that occurs in the island model for $\gamma>-1$, focusing on the steady state. The effects of migration on the dynamics of strain i on island α are readily included in the DMFT analyses. There is an additional self-consistency condition that $\bar{\nu}_i(t)$ indeed equals the average abundance of strain i over the I islands. Since the out-of-sync chaos on each island has similar properties, in steady state, the island average is equal to the time average on each island: $\langle\nu_i\rangle=\bar{\nu}_i$. A strain's invasion growth rate—its bias—is also the same on each island. The bias, $\xi_i=\langle\zeta_i\rangle-\langle\Upsilon\rangle$ (with $s_i=0$), incorporates the effect of the stabilizing term, $\Upsilon(t)$. This is essentially constant for very large K and must be positive to counteract the weaker response feedback for $\gamma>-1$, described in *Diverging Fluctuations for Near-Antisymmetric Interactions*. Since the distribution of the average drives, $\langle\zeta_i\rangle$, across the strains is Gaussian with zero mean, less than half the strains have positive ξ_i, but, nevertheless, a large majority of them persist.

Strains with large positive biases have dynamics that are minimally affected by the small rates of migration and are quantitatively similar to the ASM. In particular, the statistics of the peaks will be similar and produce correlation, $C(t-t')$, and response, $R(t-t')$, functions with the same form as for the single-island ASM. The power-law decay in correlations, $C(t-t')\sim|t-t'|^{-2/3}$, again results in a superdiffusive random walk of $\log\nu_i(t)$ when away from the peaks.

The magnitude of the chaos on each island can, as for the ASM, be characterized by a logarithmic scale, Θ. However, in contrast to the ASM, Θ, has a unique value in the spatiotemporally chaotic state. This can be estimated from marginal strains with biases near zero. With no bias, their log abundances will spread out roughly uniformly on a logarithmic scale from the peaks down to the migration floor: thus, over a range $\log(\nu^{\mathrm{peak}}/\nu^{\mathrm{mig}})\approx M\equiv\log(1/m\sqrt{K})$. This suggests that peaks occur a fraction $1/M$ of the time and that they reach a peak abundance $\nu\sim M/K$ so that the average abundances of the marginal strains are $\bar{\nu}\sim1/K$, as expected. Thus, many of the properties are similar to the ASM state with a particular temperature $\Theta\sim M$. In particular, the peak and equilibration times are $\tau_{\mathrm{peak}}\sim\sqrt{K/M}$ and $\tau_{\mathrm{eq}}\sim M\sqrt{K}$. Much of our analysis is for $1\ll M\ll K$, for which the DMFT is valid and abundances are distributed over a large log range. (In our simulations, however, even for quite large K, only a few strains may be abundant at each time, but averaging over the duration of blooms, during which many strains will peak, is roughly consistent with the DMFT results.)

Persistence and Averages with Many Islands. In the limit of infinitely many islands, in steady state, the island average $\bar{\nu}_i$ is constant and equals the single-island time average $\langle\nu_{i,\alpha}\rangle$. By assuming a value for $\bar{\nu}_i$ and solving for $\langle\nu_{i,\alpha}\rangle$ using the local DMFT equations, one can find the self-consistent solution

$\bar{\nu}_i = \langle \nu_{i,\alpha} \rangle$. There are two possibilities: globally extinct strains with $\bar{\nu}_i = 0$ and persistent strains with $\bar{\nu}_i > 0$.

The dependence of the island average on the bias ξ_i is most readily understood quantitatively for strains with either much larger than typical biases, $\xi_i \gg \hat{r}$, or large negative biases, $(-\xi_i) \gg \hat{r}$. For large positive biases, the effects of migration are small, and the island average is $\bar{\nu}_i \approx \xi_i/(-\gamma)\chi + \mathcal{O}(m)$, obtained by time-averaging $d\log(\nu_i)/dt$, as for the single-island ASM. For positive biases, this compares well to $\bar{\nu}(\xi)$, shown in Fig. 6. From the numerical simulations, the average drive $\langle \zeta_i \rangle$, and thus the biases, are inferred from the time-averaged interactions, $\sum_j V_{ij} \langle \nu_j \rangle$, which are equal to $\langle \zeta_i \rangle + \gamma\chi \langle \nu_i \rangle$ in DMFT. Thus, the static response χ can be inferred numerically from the expectation that the median (over i) of the inferred $\langle \zeta_i \rangle$ is zero, as expected with the extinct strains included.

For strains with large negative biases, abundances typically hover around the migration floor at $\nu_i^{\mathrm{mig}} = m\bar{\nu}_i/\hat{r}$. The island average is determined by the probability of rare blooms from ν_i^{mig} to large abundance. The self-consistency condition can be stated in terms of the probability density, $\rho_{\mathrm{bloom}}(\Delta\ell|\xi_i, \bar{\nu}_i)$, for a bloom that increases the log abundance by an amount $\Delta\ell$:

$$\langle \nu_i \rangle = \frac{m\bar{\nu}_i}{\hat{r}} \int e^{\Delta\ell} \rho_{\mathrm{bloom}}(\Delta\ell|\xi_i, \bar{\nu}_i)\, d\Delta\ell. \qquad [11]$$

The structure of large blooms is complex, as they will consist of a number of peaks, all of which can contribute substantially. But the dominant small factor determining ρ_{bloom} for large $\Delta\ell$ can be estimated from a large deviation analysis, carried out in *SI Appendix*, section 5.A. The power-law correlations of the drive $\eta_i(t)$ results in

$$\rho_{\mathrm{bloom}}(\Delta\ell \mid \xi_i, \bar{\nu}_i) \sim \frac{1}{M} \exp\left[-c \left(\frac{\Delta\ell}{M} \right)^{2/3} \left(\frac{-\xi_i}{\hat{r}} \right)^{4/3} \right], \qquad [12]$$

with c (here and henceforth) an order unity coefficient. We have dropped multiplicative powers of $-\xi_i/\hat{r}$, but have included $1/M$ for normalization.

It would appear that the integral in Eq. **11** diverges at large $\Delta\ell$, since ρ_{bloom} decays subexponentially with $\Delta\ell$, while the abundance reached grows exponentially with $\Delta\ell$. However, the blooms are limited to $\nu_i \sim M/K$ by the response from the other strains and, thus, have $\Delta\ell_i^{\max} \approx M + \log(M/K\bar{\nu}_i)$. This introduces a nonlinearity in $\langle \nu_i \rangle$ as a function of $\bar{\nu}_i$ that yields a solution to the self-consistent equality of these. The maximal blooms dominate the time averages, and hence the island averages. For small migration rates and nearly all strains, the $\log(M)$ term is negligible, and $\Delta\ell_i^{\max} \approx M$: the self-consistent island average is thus

$$\bar{\nu}_i \sim \frac{1}{K} \exp[-c(-\xi_i/\hat{r})^{4/3}]. \qquad [13]$$

Plots of $\bar{\nu}(\xi)$ in Fig. 6 show this roughly exponential dependence for negative ξ.

The negative biases are typically of order $\hat{r}$, so most strains have substantial average abundances. This is the result of a balance that occurs on the timescale $\tau_{\mathrm{eq}} \sim M/\hat{r}$, over which blooms last. Over a time τ_{eq}, the contributions to the change of $\log \nu_i$ due to the power-law-correlated random drive $\eta_i(t)$ and due to the bias ξ_i are both of order M. So the probability of blooms with $\Delta\ell = M$ is not very small unless the bias is anomalously negative. An important point is that M drops out of the statistics of the blooms: thus, much of the behavior is only very weakly dependent on the migration rate—especially as M itself depends only logarithmically on m. In particular, the fraction of persistent strains, shown in Fig. 3, attains a similar, large value over a broad range of migration rates, even with only modest total population per island $N = 10^9$. But at high migration rates, the persistent fraction plummets as the chaos becomes synchronized across islands.

An analysis of very negative biases in *SI Appendix*, section 5.A shows that for M large, in principle, only a very small fraction of order $\exp(-cM^2)$ of strains go globally extinct when both N and I are infinite (numerically, less than 1% go extinct for $\gamma = -0.8$ and $m/\hat{r} = 10^{-4}$, near the maximum seen in Fig. 6). But, in practice, the least abundant persistent strains will easily be driven extinct by either finite-population-size, or finite-number-of-islands, fluctuations. Most simply, when the migration rate is very low, the migration floor of many strains drops below the extinction threshold, and the persistent fraction drops (even in the large I limit), as seen in Fig. 3.

We next analyze the collective fluctuations that can lead to global extinctions when the number of islands is finite.

Global Extinctions. With a finite number of islands, the island average, $\bar{\nu}_i(t)$, fluctuates in time. With enough islands, the bloom probability is well sampled, and the fluctuations around the infinite island average, $\bar{\nu}_i^{\infty}$, are small. Even with infinite population size on each island, a strain must usually be blooming on at least one island to prevent $\bar{\nu}_i(t)$ from exponentially decreasing to global extinction. There is a critical bias, $\xi^{\mathrm{crit}} < 0$, needed for persistence: ξ^{crit} depends on the number of islands. The existence of a critical bias can already be seen in a simple toy model of two islands, as analyzed in *SI Appendix*, section 5.B and discussed in parallel work (62). In simulations, for 10 islands, ξ^{crit} is sufficiently negative that a majority of strains persist over a wide range of m and γ.

When the population size on each island is finite, the migration floor, $\nu_i^{\mathrm{mig}}(t) = m\bar{\nu}_i(t)/\hat{r}$, of strains that would otherwise persist indefinitely can, by chance, fluctuate down to $1/N$, leading to a series of local, and possibly global, extinctions. A general downward drift of $\log(\nu_i^{\mathrm{mig}})$ is interspersed with recoveries by blooms. Extinction requires an extended period during which blooms fail to reach log-abundance changes of $\Delta\ell \gtrsim M$ which are needed to increase ν_i^{mig}.

The extinction probability for a strain can be estimated heuristically from its bloom probability. An unlucky fluctuation of the

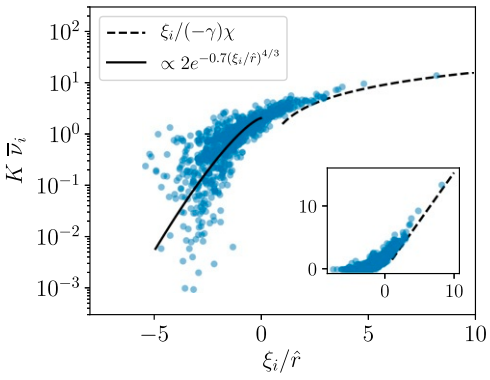

Fig. 6. Island-average abundances vs. bias. Mean-field analysis predicts the relationship between abundances of strains (shown on log scale) and their biases ξ_i, their average growth rate at low abundance on a single island. (*Inset*) Same plot on linear scale. Theoretical predictions for ξ_i substantially positive (dotted line) and substantially negative (solid line) agree reasonably well with the numerics. Data are shown for the long-term persistent strains for $\gamma = -0.8$, $K = 100$, $m/\hat{r} = 2 \cdot 10^{-8}$ ($M = 18$), and $I = 24$ islands. The dependence of $\bar{\nu}$ on ξ is largely independent of I, although fewer strains survive for smaller I.

migration floor from $\nu^{\text{mig}} \sim m/K\hat{r}$ down to $1/N$ takes a time $\Delta t_{\text{ext}} \sim \log(Nm/K\hat{r})/\hat{r}$. (The nature of the least unlikely such fluctuation is analyzed in *SI Appendix*, section 5.C.) Blooms of sufficient size for recovery ($\Delta\ell \gtrsim M$) occur at a rate $\sim \rho_{\text{bloom}}(M|\xi_i)/\tau_{\text{eq}}$, with $\tau_{\text{eq}} \sim M/\hat{r}$ and the bloom probability (for negative ξ_i) given by Eq. **12**. Given that blooms on different islands, or at well-separated times, are roughly independent, the probability of extinction happening when no large blooms occur for a time Δt_{ext} is

$$\log\left[p_{\text{ext}}(\xi_i)\right] \sim -I\rho_{\text{bloom}}(M|\xi_i)\frac{\log(Nm/K\hat{r})}{M} \equiv -I/I_X(\xi_i), \quad [14]$$

up to unknown powers of $(-\xi/\hat{r})$. Thus, how long a strain persists before global extinction depends strongly on its ξ_i: $T_i^{\text{persist}} \sim \exp(I/I_X(\xi_i))$. With many islands, most persistent strains will survive for exponentially long times, with some marginal strains going extinct much more quickly. Plotting the fraction of initial strains that have gone extinct vs. time (Fig. 5) shows that, even with a modest number of islands, many strains survive for very long periods of time. The exponential dependence on I can be seen explicitly by plotting the kth extinction time as a function of I (Fig. 5, *Inset*).

Discussion

We have shown that antisymmetric correlations in the LV interaction matrix, together with simple spatial structure, are sufficient to stabilize extensive diversity of an assembled community. No niche-like assumptions or special properties are needed. This spatiotemporally chaotic "phase" is very robust; the key ingredient is the negative feedback induced by the antisymmetric correlations and sufficient—albeit very small—migration. While some fraction of the strains go deterministically extinct, a majority persist for very long times. This includes—crucially—strains with substantially negative average growth rate, which, in a well-mixed population, would guarantee their extinction. The key to their persistence with spatial structure is that each strain occasionally has a local bloom to high abundance which provides migrants to the other islands. As these blooms are nearly independent from island to island, global extinctions occur only if blooms do not happen on any of the islands for a sufficiently long period. This makes the spatiotemporally chaotic phase very stable, even for modest numbers of islands.

Much of our analysis has focused on the asymptotic, but unrealistic, regime when logarithmic functions of the population size and the migration rate are large. This has enabled us to obtain many results in a general framework based on DMFT. Yet our simulations show that the predicted behaviors are correct, even semiquantitatively, for modest sizes of parameters. A crucial prediction is the exponential scaling of survival times with the number of islands, illustrated in Fig. 5, for realistic parameters: total population per island, $N \approx 10^{13}$—of order the number of human gut bacteria (66)—and $K = 100$ strains.

Generalizations. The diverse spatiotemporally chaotic phase should exist far beyond the models we have analyzed. In *SI Appendix*, section 6, we discuss the behavior of the general random LV model with niche-like interactions (parameterized by $Q = -V_{ii}$) and argue that the spatiotemporally chaotic phase exists over much of the $\gamma - Q$ phase diagram. With selective differences s_i, the bias, ξ_i, for each strain includes both this and the effects of interactions, although its behavior only depends on the sum of the two parts. However, the statistical properties of the spatiotemporal state—including the distribution across strains of the contribution of the interactions to ξ_i—depends on the distribution of the s_i. This causes the number of persistent strains to decrease substantially when $\text{Var}[s_i] \geq \mathcal{O}(1/K)$, as analyzed in *SI Appendix*, section 3.B. But the qualitative behavior is unchanged.

More generally, the spatiotemporally chaotic phase should exist with sparse interactions, broad distributions of interaction strengths, correlations due to phylogenetic relatedness of strains, or with some variations between islands. Indeed, even overall antisymmetric correlations of the interactions are not essential. The key is the absence of strains that always outcompete most other strains, and that, for each strain, there are some ecological interactions that provide negative feedback, preventing it from persisting at high abundance. We showed how this occurs for antisymmetrically correlated interactions, but this can also occur with moderately strong niche-like competition with its own strain ($Q = \mathcal{O}(\sqrt{K})$) combined with sufficiently random interactions with many other strains. Indeed, in parallel work, Roy et al. (62, 67) have found, for $\gamma = 0$ (independent V_{ij}), a chaotic phase stabilized by migration with behavior consistent with our predictions.

Extrinsically driven chaos. Dynamics with large swings of local abundances are crucial for stabilizing the spatiotemporally chaotic phase. But these need not be driven primarily by complex ecology. Extrinsic spatiotemporal environmental fluctuations, to which different strains respond differently, can cause blooms on different islands roughly independently. Blooms will be limited by the overall carrying capacity on each island, but no strain-specific interactions are needed. Migration can then stabilize the coexistence of diverse strains, even if they do badly on average, i.e., with time-averaged fitness, analogous to their ξ_i, negative. This is a recognized mechanism for promoting species coexistence, known as the "spatial storage effect" (47). The behavior is in striking contrast to that of a well-mixed population in a fluctuating environment whose time-averaged fitness must be positive to avoid extinctions. With spatiotemporal variations in fitness together with migration, a strain is characterized by its *global*-invasion eigenvalue (as analyzed for two islands in *SI Appendix*, section 5.B). When its global-invasion eigenvalue is positive, a strain can invade from low abundance and persist (47).

Although much of the behavior is similar, there is a crucial distinction between chaotic dynamics driven by intrinsic ecological interactions between multiple strains and that driven by extrinsic spatiotemporal variations. For ecologically driven chaos, the magnitude of the dynamical variations in growth rates relative to their averages "self-tunes" the statistics of blooms to yield stable coexistence. Such a balance will generally not occur for extrinsically driven spatiotemporal chaos: extensive coexistence will depend sensitively on parameters and is by no means assured. [Indeed, it has been shown that the storage effect's contribution to the global invasion eigenvalue decreases with the number of strains (47).]

In general, environmental variations will occur alongside complex ecological interactions. And the resulting behavior can be complicated; see, for example, ref. 68. But the analytical methods developed in this paper for treating the dynamics of multiple strains should be useful for developing more general understanding of the complex interplay of predation, competition, and environmental fluctuations.

Abundance distributions. A key quantitative characteristic of the spatiotemporal chaos is a general consequence of the dramatic fluctuations of local populations. "Snapshots" of the local abundances will be broadly distributed on a logarithmic scale (Fig. 4). How universal are such abundance distributions? At low abundance, they will be affected by details of migration, while at high abundance, different mechanisms for limiting blooms (*SI Appendix*, section 6), such as strong niche-like interactions, or some strains doing atypically well on average (*SI Appendix*, section 3.B), will change the abundance distribution. But the wide intermediate range of abundances will be far more universal—with dynamics like the seemingly special perfectly antisymmetric model! The lack of universality at both

high and low abundance means that summary statistics like the "Shannon diversity" (entropy of the distribution) or "species richness" (total number of strains observed) are poor characterizations of the abundance distributions: the former is dominated by high-abundance strains and the latter by very-low-abundance strains.

The more universal intermediate part of the abundance distribution will be approximately a power law with exponent one. This is the same as from the neutral theory of ecology (31). In fact, a neutral model with immigration from a mainland at strain-dependent rates $\mu_i = \frac{K}{\Theta N}\bar{\nu}_i$ has an identical joint distribution of abundances as the ASM with "temperature" Θ and mean fractional abundances, $\bar{\nu}_i$. But the underlying dynamics are very different, qualitatively and quantitatively, especially for large microbial populations, for which birth–death fluctuations are usually negligible. Many ecosystems exhibit broad abundance distributions which are used to argue for or against different ecological scenarios (13). But our work surely implies that sampling at one location and time is far from sufficient: spatiotemporal data—by time series from deep sequencing—are needed to distinguish between scenarios (69).

Bacteria-phage strain-level diversity. The most natural context for antisymmetric correlations in the interactions between multiple types is diverse strains of both a host species and a generalist pathogen species, especially bacteria and phage. Models of such systems with perfectly antisymmetric ($\gamma = -1$) interactions have been studied, but with only tens of strains (70–72). Dynamical mean-field analysis in *SI Appendix*, section 4 enables understanding of large numbers of strains with broad, randomly varying infectivity. The primary additional parameter is the ratio of timescales over which the differences between strains result in substantial abundance changes for the bacterial strains vs. that for the phage strains. If these ecological timescales are identical, the mean-field dynamics of both the bacterial and phage strains is identical to the ASM. If the timescales differ substantially, we expect quantitative, but not qualitative, differences. Spatial structure obviates the need for perfect antisymmetry—unrealistic in any case—and our scenario and analysis of a spatiotemporally chaotic phase should hold for generalist bacteria-phage models.

Dynamical diversity from bacteria–phage interactions has recently been studied by other approaches. For example, some explicit kill-the-winner models treat phage predation as stochastic events leading to bacterial population collapse (73). While these exhibit persistent diversity, it is unclear whether there is a reasonable underlying population dynamics that could give rise to the caricature used. The advantage of models with explicit population dynamics for bacteria and phage is that avoidance of extinctions cannot be put in "by hand." Furthermore, models of the strain interactions as we have studied naturally allow for nonspecific interactions, instead of the one-bacteria-one-phage scenario of the original kill-the-winner models (52, 53, 74), which is destabilized by demographic stochasticity. Indeed, nonspecific interactions may well be needed to stabilize a chaotic phase (75).

Extensions. Our conceptual and analytical frameworks should enable biologically relevant extensions in various directions.

Realistic spatial structure. The effects of real spatial structure surely merit exploration. With conditions being the same everywhere, but transport either by local diffusion or occasional long-distance dispersal by wind, ocean currents, or hitchhiking on animals (76), the process of recovering from local extinctions is more complex, as it must involve spatial propagation of repopulation "fronts." With a small number of strains having cyclic "rock–paper–scissors" interactions, spatiotemporally chaotic coexistence has been shown with repopulation fronts taking the form of spiral waves. With many similar strains, can a substantial fraction survive globally in a chaotic state, even in a system of infinite spatial extent?

Microbial spores or "seedbanks." When faced with unfavorable environmental conditions, many microbes enter a reversible state of dormancy by forming spores or other resting structures (77). The formation of long-lived—but not immortal—spores is another mechanism that can stabilize a diverse ecologically chaotic phase—indeed, even in a well-mixed system with no spatial structure. If some fraction of each strain forms spores that die off slowly, but occasionally germinate to produce actively dividing cells, the spore population effectively averages the chaotic dynamics of the active cell populations over time. This is analogous to averaging over a set of islands. For populations with large fluctuations driven by extrinsic environmental variations, this is the temporal "storage effect" (46). The product of the average spore lifetime, τ_{sp}, and the typical invasion growth rates, $\hat{r}$, of the active cell populations is roughly equivalent to the number of islands. With deterministic dynamics and statistics of interactions similar to those we have studied, a substantial fraction of the strains will survive forever. Even with spore extinctions, the survival times will be exponentially long in the spore lifetime, including for strains whose bias—average growth rate of the germinated population, ξ_i—is negative. Individual strains will persist for time $T^{\text{persist}} \sim \exp[A(\xi)\hat{r}\tau_{sp}]$ with $A(\xi)$, depending also on the population size of the spores, the germination rate, and other factors. Thus, even spores with moderate lifetimes can yield a diverse chaotic ecology, with many strains having negative average growth rate, but surviving for extremely long times.

Phenotype models. An unsatisfactory feature of LV models of many interacting strains is that the organisms do not interact via their phenotypic properties: their phenotype is defined by their interactions with others. There is a long history of more explicit phenotype modeling for species interacting via consumption of common resources—MacArthur consumer resource models and generalizations (18–21, 78). More generally, one can consider interactions via many chemicals in the environment, with the dynamics of the populations set by the chemical concentrations and the dynamics of the chemical concentrations set by the population sizes of the various strains. Our analysis should be readily extendable to at least simple versions of such models, most simply when they reduce to LV models, with interactions determined by the effect of one strain on the environment and the response of the other strain to this. Under what conditions will a spatiotemporally chaotic phase exist in ecological models with interactions only via modifications of the environment? And how much diversity can be stabilized by the interplay between chaos and migration? This is a productive avenue for future research. A more general question is how systems will behave with direct interaction between pairs of individuals—and thus, again, LV structure—but with the interactions determined by phenotypic properties of the two organisms (rather than an abstract V_{ij}).

Evolution and ecology. We have studied how a large number of closely related strains can coexist when assembled together, but can such communities of strains be evolved in the first place? Although for microbial populations, there is usually no clear separation between ecological and evolutionary timescales, coexisting strains are found to have a wide spectrum of genetic differences and, hence, times to their common ancestors. The most basic case—and the hardest scenario for extensive diversity to exist—is when evolution is the slowest process. In simple models of assembled communities, mutations to new strains can lead to collapse (78) or to buildup of diversity (79, 80), depending on how the new mutants' interactions are modeled. Eco–evo models should characterize the strains by phenotypic properties, which are what evolves, and the interactions be determined by these, without strict tradeoffs [which are often assumed (20, 81)]. In an

already-evolved population, there are likely few generalist mutations (higher s_i) available, but many more potential mutations that take advantage of the particular combination of strains in the system at the time and location at which they arise.

Can a highly diverse chaotic community evolve in general phenotype-based models? If so, will the system undergo continual Red Queen evolution with no systematic "improvement"? Or will the evolution tend to get slower and slower? The statistical properties conditioned on evolution will likely be quite different from those in an assembled community, described in ref. 26. What general features might emerge? And how might different scenarios—and different possible "phases" of the eco–evo dynamics—potentially be distinguished by data from real microbial populations?

Data Availability Statement. This is a purely theoretical paper; there are no data associated with it.

ACKNOWLEDGMENTS. A.A. was supported by a Bowes BioX fellowship and Stanford's Center for Computational, Evolutionary, and Human Genomics. M.T.P. was supported by William R. and Sara Hart Kimball as a Stanford Graduate Fellow and by NSF Graduate Research Fellowship. DGE-114747. All authors were supported by NSF Grant PHY-1607606. We thank Giulio Biroli, Felix Roy, and Guy Bunin for valuable discussions and sharing the results of their parallel work. Computer resources were provided by the Stanford Research Computing Center's Sherlock cluster.

1. G. E. Hutchinson, The paradox of the plankton. *Am. Nat.* **95**, 137–145 (1961).
2. S. G. Acinas *et al.*, Fine-scale phylogenetic architecture of a complex bacterial community. *Nature* **430**, 551–554 (2004).
3. M. J. Rosen, M. Davison, D. Bhaya, D. S. Fisher, Fine-scale diversity and extensive recombination in a quasisexual bacterial population occupying a broad niche. *Science* **348**, 1019–1023 (2015).
4. M. J. Rosen, M. Davison, D. S. Fisher, D. Bhaya, Probing the ecological and evolutionary history of a thermophilic cyanobacterial population via statistical properties of its microdiversity. *PLoS One* **13**, e0205396 (2018).
5. J. Oh *et al.*, Biogeography and individuality shape function in the human skin metagenome. *Nature* **514**, 59–64 (2014).
6. J. Oh, A. Byrd, M. Park, H. Kong, J. Segre, Temporal stability of the human skin microbiome. *Cell* **165**, 854–866 (2016).
7. M. Tikhonov, R. W. Leach, N. S. Wingreen, Interpreting 16S metagenomic data without clustering to achieve sub-OTU resolution. *ISME J.* **9**, 68–80 (2015).
8. N. R. Garud, B. H. Good, O. Hallatschek, K. S. Pollard, Evolutionary dynamics of bacteria in the gut microbiome within and across hosts. *PLoS Biol.* **17**, e3000102 (2019).
9. S. J. Biller, P. M. Berube, D. Lindell, S. W. Chisholm, Prochlorococcus: The structure and function of collective diversity. *Nat. Rev. Microbiol.* **13**, 13–27 (2015).
10. N. Kashtan *et al.*, Single-cell genomics reveals hundreds of coexisting subpopulations in wild Prochlorococcus. *Science* **344**, 416–420 (2014).
11. F. M. Cohan, E. B. Perry, A systematics for discovering the fundamental units of bacterial diversity. *Curr. Biol.* **17**, R373–R386 (2007).
12. M. D. J. Lynch, J. D. Neufeld, Ecology and exploration of the rare biosphere. *Nat. Rev. Microbiol.* **13**, 217–229 (2015).
13. E. Ser-Giacomi *et al.*, Ubiquitous abundance distribution of non-dominant plankton across the global ocean. *Nat. Ecol. Evol.* **2**, 1243–1249 (2018).
14. A. Shade *et al.*, Conditionally rare taxa disproportionately contribute to temporal changes in microbial diversity. *mBio* **5**, e01371–14 (2014).
15. F. d'Ovidio, S. De Monte, S. Alvain, Y. Dandonneau, M. Lévy, Fluid dynamical niches of phytoplankton types. *Proc. Natl. Acad. Sci. U.S.A.* **107**, 18366–18370 (2010).
16. P. Chesson, Mechanisms of maintenance of species diversity. *Annu. Rev. Ecol. Systemat.* **31**, 343–366 (2000).
17. R. MacArthur, Species packing and competitive equilibrium for many species. *Theor. Popul. Biol.* **1**, 1–11 (1970).
18. P. Chesson, MacArthur's consumer-resource model. *Theor. Popul. Biol.* **37**, 26–38 (1990).
19. D. Tilman, Resource competition and community structure. *Monogr. Popul. Biol.* **17**, 1–296 (1982).
20. M. Tikhonov, R. Monasson, Collective phase in resource competition in a highly diverse ecosystem. *Phys. Rev. Lett.* **118**, 048103 (2017).
21. M. Advani, G. Bunin, P. Mehta, Statistical physics of community ecology: A cavity solution to MacArthur's consumer resource model. *J. Stat. Mech. Theor. Exp.* **2018**, 033406 (2018).
22. R. M. May, Will a large complex system be stable?. *Nature* **238**, 413–414 (1972).
23. S. Diederich, M. Opper, Replicators with random interactions: A solvable model. *Phys. Rev. A* **39**, 4333–4336 (1989).
24. T. Galla, Random replicators with asymmetric couplings. *J. Phys. Math. Gen.* **39**, 3853–3869 (2006).
25. Y. Yoshino, T. Galla, K. Tokita, Statistical mechanics and stability of a model eco-system. *J. Stat. Mech. Theor. Exp.* **2007**, P09003 (2007).
26. G. Bunin, Ecological communities with Lotka-Volterra dynamics. *Phys. Rev. E* **95**, 042414 (2017).
27. G. Biroli, G. Bunin, C. Cammarota, Marginally stable equilibria in critical ecosystems. *New J. Phys.* **20**, 083051 (2018).
28. S. P. Hubbell, *The Unified Neutral Theory of Biodiversity and Biogeography* (Monographs in Population Biology, Princeton University Press, Princeton, NJ, 2001), vol. MPB-32.
29. S. P. Hubbell, Neutral theory and the evolution of ecological equivalence. *Ecology* **87**, 1387–1398 (2006).
30. J. Rosindell, S. P. Hubbell, R. S. Etienne, The unified neutral theory of biodiversity and biogeography at age ten. *Trends Ecol. Evol.* **26**, 340–348 (2011).
31. I. Volkov, J. R. Banavar, S. P. Hubbell, A. Maritan, Neutral theory and relative species abundance in ecology. *Nature* **424**, 1035–1037 (2003).
32. S. Pueyo, Diversity: Between neutrality and structure. *Oikos* **112**, 392–405 (2006).
33. I. Volkov, J. R. Banavar, S. P. Hubbell, A. Maritan, Patterns of relative species abundance in rainforests and coral reefs. *Nature* **450**, 45–49 (2007).
34. S. Nee, The neutral theory of biodiversity: Do the numbers add up?. *Funct. Ecol.* **19**, 173–176 (2005).
35. M. Danino, N. M. Shnerb, S. Azaele, W. E. Kunin, D. A. Kessler, The effect of environmental stochasticity on species richness in neutral communities. *J. Theor. Biol.* **409**, 155–164 (2016).
36. M. Kalyuzhny, R. Kadmon, N. M. Shnerb, A neutral theory with environmental stochasticity explains static and dynamic properties of ecological communities. *Ecol. Lett.* **18**, 572–580 (2015).
37. R. M. May, Simple mathematical models with very complicated dynamics. *Nature* **261**, 459–467 (1976).
38. A. Hastings, C. L. Hom, S. Ellner, P. Turchin, H. C. J. Godfray, Chaos in ecology: Is mother nature a strange attractor?. *Annu. Rev. Ecol. Systemat.* **24**, 1–33 (1993).
39. J. Huisman, F. J. Weissing, Biodiversity of plankton by species oscillations and chaos. *Nature* **402**, 407–410 (1999).
40. M. Scheffer, Should we expect strange attractors behind plankton dynamics—and if so, should we bother?*J. Plankton Res.* **13**, 1291–1305 (1991).
41. E. Benincà *et al.*, Chaos in a long-term experiment with a plankton community. *Nature* **451**, 822–825 (2008).
42. B. Rodriguez-Brito *et al.*, Viral and microbial community dynamics in four aquatic environments. *ISME J.* **4**, 739–751 (2010).
43. B. J. Campbell, L. Yu, J. F. Heidelberg, D. L. Kirchman, Activity of abundant and rare bacteria in a coastal ocean. *Proc. Natl. Acad. Sci. U.S.A.* **108**, 12776–12781 (2011).
44. I. Ispolatov, V. Madhok, S. Allende, M. Doebeli, Chaos in high-dimensional dissipative dynamical systems. *Sci. Rep.* **5**, 12506 (2015).
45. J. B. T. Sanders, J. D. Farmer, T. Galla, The prevalence of chaotic dynamics in games with many players. *Sci. Rep.* **8**, 4902 (2018).
46. P. Chesson, Multispecies competition in variable environments. *Theor. Popul. Biol.* **45**, 227–276 (1994).
47. P. Chesson, General theory of competitive coexistence in spatially-varying environments. *Theor. Popul. Biol.* **58**, 211–237 (2000).
48. J. C. Allen, W. M. Schaffer, D. Rosko, Chaos reduces species extinction by amplifying local population noise. *Nature* **364**, 229–232 (1993).
49. G. D. Ruxton, Low levels of immigration between chaotic populations can reduce system extinctions by inducing asynchronous regular cycles. *Proc. Roy. Soc. Lond. B Biol. Sci.* **256**, 189–193 (1994).
50. F. Rodriguez-Valera *et al.*, Explaining microbial population genomics through phage predation. *Nat. Rev. Microbiol.* **7**, 828–836 (2009).
51. K. Vetsigian, R. Jajoo, R. Kishony, Structure and evolution of streptomyces interaction networks in soil and in silico. *PLoS Biol.* **9**, e1001184 (2011).
52. T. F. Thingstad, Elements of a theory for the mechanisms controlling abundance, diversity, and biogeochemical role of lytic bacterial viruses in aquatic systems. *Limnol. Oceanogr.* **45**, 1320–1328 (2000).
53. C. Winter, T. Bouvier, M. G. Weinbauer, T. F. Thingstad, Trade-offs between competition and defense specialists among unicellular planktonic organisms: The "killing the winner" hypothesis revisited. *Microbiol. Mol. Biol. Rev.* **74**, 42–57 (2010).
54. J. Vandermeer, Coupled oscillations in food webs: Balancing competition and mutualism in simple ecological models. *Am. Nat.* **163**, 857–867 (2004).
55. J. Vandermeer, Oscillating populations and biodiversity maintenance. *Bioscience* **56**, 967–975 (2006).
56. K. Holmfeldt, M. Middelboe, O. Nybroe, L. Riemann, Large variabilities in host strain susceptibility and phage host range govern interactions between lytic marine phages and their flavobacterium hosts. *Appl. Environ. Microbiol.* **73**, 6730–6739 (2007).
57. J. S. Weitz *et al.*, Phage–bacteria infection networks. *Trends Microbiol.* **21**, 82–91 (2013).
58. N. S. Goel, S. C. Maitra, E. W. Montroll, On the Volterra and other nonlinear models of interacting populations. *Rev. Mod. Phys.* **43**, 231–276 (1971).
59. R. Macarthur, R. Levins, The limiting similarity, convergence, and divergence of coexisting species. *Am. Nat.* **101**, 377–385 (1967).
60. T. Chawanya, K. Tokita, Large-dimensional replicator equations with antisymmetric random interactions. *J. Phys. Soc. Jpn.* **71**, 429–431 (2002).
61. M. Vallade, B. Houchmandzadeh, Analytical solution of a neutral model of biodiversity. *Phys. Rev. E* **68**, 061902 (2003).
62. F. Roy, G. Biroli, G. Bunin, C. Cammarota, Numerical implementation of dynamical mean field theory for disordered systems: Application to the Lotka-Volterra model of ecosystems. *J. Phys. A: Math. Theor.* **52**, 484001 (2019).

63. R. H. MacArthur, E. O. Wilson, *The Theory of Island Biogeography* (Princeton University Press, Princeton, NJ, 1967).
64. A. Pikovsky, M. Rosenblum, J. Kurths, *Synchronization: A Universal Concept in Nonlinear Sciences* (Cambridge Nonlinear Science Series, Cambridge University Press, Cambridge, UK, 2001), vol. 12.
65. H. Sompolinsky, A. Zippelius, Relaxational dynamics of the Edwards-Anderson model and the mean-field theory of spin-glasses. *Phys. Rev. B* **25**, 6860–6875 (1982).
66. R. Sender, S. Fuchs, R. Milo, Revised estimates for the number of human and bacteria cells in the body. *PLoS Biol.* **14**, e1002533 (2016).
67. F. Roy, M. Barbier, G. Biroli, G. Bunin, Can endogenous fluctuations persist in high-diversity ecosystems? *PLoS Comput. Biol.* **16**, e1007827 (2020).
68. J. J. Kuang, P. Chesson, Interacting coexistence mechanisms in annual plant communities: Frequency-dependent predation and the storage effect. *Theor. Popul. Biol.* **77**, 56–70 (2010).
69. B. J. McGill *et al.*, Species abundance distributions: Moving beyond single prediction theories to integration within an ecological framework. *Ecol. Lett.* **10**, 995–1015 (2007).
70. L. F. Jover, M. H. Cortez, J. S. Weitz, Mechanisms of multi-strain coexistence in host–phage systems with nested infection networks. *J. Theor. Biol.* **332**, 65–77 (2013).
71. J. S. Weitz, H. Hartman, S. A. Levin, Coevolutionary arms races between bacteria and bacteriophage. *Proc. Natl. Acad. Sci. U.S.A.* **102**, 9535–9540 (2005).
72. H. T. Williams, Phage-induced diversification improves host evolvability. *BMC Evol. Biol.* **13**, 17 (2013).
73. S. Maslov, K. Sneppen, Population cycles and species diversity in dynamic Kill-the-Winner model of microbial ecosystems. *Sci. Rep.* **7**, 39642 (2017).
74. T. F. Thingstad, S. Våge, J. E. Storesund, R. A. Sandaa, J. Giske, A theoretical analysis of how strain-specific viruses can control microbial species diversity. *Proc. Natl. Acad. Sci. U.S.A.* **111**, 7813–7818 (2014).
75. C. Xue, N. Goldenfeld, Coevolution maintains diversity in the stochastic "kill the winner" model. *Phys. Rev. Lett.* **119**, 268101 (2017).
76. O. Hallatschek, D. S. Fisher, Acceleration of evolutionary spread by long-range dispersal. *Proc. Natl. Acad. Sci. U.S.A.* **111**, E4911–E4919 (2014).
77. J. T. Lennon, S. E. Jones, Microbial seed banks: The ecological and evolutionary implications of dormancy. *Nat. Rev. Microbiol.* **9**, 119–130 (2011).
78. N. Shoresh, M. Hegreness, R. Kishony, Evolution exacerbates the paradox of the plankton. *Proc. Natl. Acad. Sci. U.S.A.* **105**, 12365–12369 (2008).
79. F. Dercole, R. Ferriere, S. Rinaldi, Chaotic Red Queen coevolution in three-species food chains. *Proc. Biol. Sci.* **277**, 2321–2330 (2010).
80. E. T. Miller, C. A. Klausmeier, Evolutionary stability of coexistence due to the storage effect in a two-season model. *Theor. Ecol.* **10**, 91–103 (2017).
81. A. Posfai, T. Taillefumier, N. S. Wingreen, Metabolic trade-offs promote diversity in a model ecosystem. *Phys. Rev. Lett.* **118**, 028103 (2017).